Retrofit for Blast- Resistant RC Slabs with Composite Materials

Binggeng Lu, Pedro Silva, Antonio Nanni, and Jason Baird

Synopsis: This research program was initiated to examine the feasibility of assessing the blast-resistant capacity of reinforced concrete (RC) slabs using the displacement based design (DBD) method. In order to achieve this objective, five RC slabs were tested under real blast loads in the out-of-plane direction. One of the slabs was used as the control unit to establish a baseline for comparison in terms of performance for the other four slabs, which were strengthened with fiber reinforced polymer (FRP) and steel fiber reinforced polymer (SRP). The explosive charge weight and stand-off distance required to impose a given damage level were predicted by the DBD method. Test results showed that the blast loads were effectively estimated and the damage levels observed from the field tests correlated well with the predicted levels. In addition, test results corroborated that the blast-resistant capacity of RC slabs can be effectively increased by strengthening using FRP composites. The main conclusion that can be drawn from these tests using improvised explosive devices (IDE) is that RC slabs retrofitted on both sides have a higher blast resistance capacity than those slabs retrofitted only on one side. This paper discusses these experimental results along with the analysis steps used to predict the blast charge and standoff distance to impose a given damage level.

Keywords: Blast-resistant; Fiber reinforced polymers; Displacement based method; Ductility; Steel reinforced polymers

Binggeng Lu is a graduate student at the Center for Infrastructure Engineering Studies (CIES) at the University of Missouri–Rolla (UMR). His research interests include the performance and evaluation of structures subjected to seismic and blast loads.

Pedro Franco Silva is an assistant professor of Civil Engineering in CIES at UMR. He received his PhD from the University of California-San Diego, Calif. His research interests include earthquake engineering and the seismic performance evaluation of bridge structures.

Antonio Nanni, FACI, is the V&M Jones Professor of Civil Engineering and Director of CIES at UMR. He is chair and member of ACI437, Strength Evaluation of Existing Concrete Structures; 440, Fiber Reinforced Polymer; Reinforcement; 544, Fiber Reinforced Concrete; 549, and Joint ACI-ASCE-TMS Committee. His research interests include performance of concrete-based structures.

Jason Baird, is a research assistant professor in the Department of Mining Engineering at UMR and the president of Loki, Inc. His research interests include blast optimization and design of blast-resistant structures.

INTRODUCTION

Recent events have drawn considerable attention to the vulnerability and sustainability of structural members subjected to improvised explosive devices (IED). Since protection is never an absolute concept and there is a level of high cost associated with a given damage level of protection, proper assessment tools must be employed to determine within a reasonable degree of accuracy the level of vulnerability of existing and new structures. Furthermore, in blast design, one must also determine an acceptable level of damage that a structure can tolerate. Explosive effects can impact a level of damage that can range from minor damage to completely structural failure and considerable loss of life (FEMA, 2003). This research program has shown promising results in using the DBD method to predict blast loads in terms of standoff distance and charge weight.

In this program, the performance of concrete slabs strengthened with carbon fiber reinforced polymers (CFRP) and a new class of composites composed of knitted high strength steel cords designated as steel reinforced polymers (SRP) (Wobbe et al., 2004) were investigated under real blast loads. Different retrofit schemes consisting of these CFRP and SRP strengthening schemes applied on one side and both sides of the tested slabs were investigated and results are discussed in this paper. In total five slabs with different strengthening schemes and materials were tested under real blast loads.

EXPERIMENTAL PROGRAM

Test Specimens

As shown in Figure 1, a series of square RC slabs with nominal dimensions of 1200 x 1200 x 89mm were chosen for the experimental and analytical investigation. Different materials and upgrade schemes were investigated against out-of-plane blast loads. Five RC slabs were built and strengthened with different schemes and different materials such as CFRP or SRP. With the exception of the control slab (1), two slabs (2A and 2B) were strengthened with CFRP laminates, and the other two (3A and 3B), were strengthened with SRP laminates. The strengthening schemes are also shown in Figure 1. Slabs 2A and 3A were strengthened on bottom side (tensile face) only, whereas, slabs 2B and 3B were strengthened on both sides to evaluate the influence of negative moments developed under the dynamic response.

The experimental specimens were tested at the experimental mine at the University of Missouri-Rolla. As shown in Figure 2a, it can be seen that the distance from the test specimen to the mine walls and ceiling are enough apart that open air design method will be applicable. As shown in Figure 2b, the test specimens were simply supported by two steel box beams. The charge was suspended above the test specimens to the specific standoff distance by a wire, which was also used as the circuit to detonate the charge. Each charge was composed of desensitized RDX high explosive.

Material Properties and Moment-Curvature Relationships

The material properties are as follows. All the five specimens were poured with 28MPa concrete and reinforced with steel bars of a 0.18% reinforcement ratio in each direction. The steel grade was 410MPa with an elastic modulus of 200GPa. The CFRP and SRP laminates demonstrated an elastic behavior up to its ultimate tensile strength, which was 3790MPa and 1170MPa, and the elastic modulus was 230GPa and 78GPa, respectively. The summary of all material properties are shown in Table 1.

The thickness of the CFRP laminates and the SRP laminates were 0.17mm and 0.48mm, respectively. In all cases the width of laminates was 1200mm. Based on the material properties, the static equivalent moment-curvature relationship for the five slabs are presented in Figure 3. In order to limit the reinforcement ratio to levels that would want testing initial the minimize scale of damage capacity, the minimum reinforcement ratio according to secondary reinforcement consideration was provided. As such the reinforcement ratio of the test slabs was 0.18%.Under the action of blast loads the effect of high rate of strain application was considered by applying a dynamic increase factor (DIF) 1.20 for reinforcement bars and 1.25 for concrete, respectively (Mays and Smith, 1995). Under the given reinforcement ratio, the yielding moment of the control slab was 7.2kN-m and the crack moment was 6.5kN-m. The moment-curvature relationships of slabs 2A and 2B are identical because the CFRP laminates on the compressive face were ignored in the analysis. For the same reason, moment-curvature relationships for slabs 3A and 3B are also identical.

PREDICTION OF BLAST LOADING

In this work, the shape of the blast pressure wave was schematically simplified as a triangle impulse loading, as shown in Figure 4 (FEMA, 2003). In this figure, the negative pressure was not considered in the analysis, but future work should include this effect. The principal parameters required to define the blast loading are the peak overpressure, P_s, and the duration of the blast impulse, t_d. Simple expressions can be used to relate these parameters to the weight of charge and the standoff distance expressed as W and R, respectively.

Blast Load Relations

The peak overpressure can be expressed as a function of Z, which is designated as the blast load scaled distance (Mays and Smith, 1995):

$$P_s = \frac{6.7}{Z^3} + 1 \quad \text{bar} \qquad (P_s \geq 10 \quad \text{bar})$$
$$P_s = \frac{0.975}{Z} + \frac{1.455}{Z^2} + \frac{5.85}{Z^3} - 0.019 \quad \text{bar} \qquad (0.1 \leq P_s \leq 10 \quad \text{bar}) \tag{1}$$

In this equation, the scaled distance, Z, is correlated to W and R by:

$$Z = \frac{R}{W^{1/3}} \tag{2}$$

In this equation, the standoff distance is measured in meters, and the charge weight is based on a TNT-mass equivalence measured in kilograms. The duration of the blast impulse, t_d, can be determined as a function of W and R, given by (Lam et al, 2004; Mays and Smith, 1995):

$$\log_{10}\left(\frac{t_d}{W^{1/3}}\right) \approx -2.75 + 0.27\log_{10}\left(\frac{R}{W^{1/3}}\right) \qquad (Z \geq 1.0)$$
$$\log_{10}\left(\frac{t_d}{W^{1/3}}\right) \approx -2.75 + 1.95\log_{10}\left(\frac{R}{W^{1/3}}\right) \qquad Z \leq 1.0 \tag{3}$$

This equation was then used to correlate the charge weight and the stand-off distance to the load duration. In the next section, prediction of the charge weight and standoff distance necessary to impose a given damage level on the tested slabs were based on the principles of the DBD method discussed next.

Displacement Based Method Applied for Prediction of Blast Loads

An attractive feature of the DBD method is that the structural performance criteria selected for design or assessment can be correlated to a measurable quantity such as the displacement ductility. For RC members, displacement ductility levels in the range of 1 to 6 can be correlated to performance damage levels that either lead to "small cracks only" or "major damage requiring repair", respectively. These performance goals have been obtained based on test results, which confirm that these performance levels can be directly related to the displacement ductility levels (Hose et al., 2000).

In applying the DBD method it is practical to convert the bilinear inelastic response of a given member to an idealized linear elastic response, as shown in Figure 5 (Priestley et al., 1995). According to this procedure the entire inelastic force-displacement response is described by an idealized linear elastic system with an equivalent stiffness, K_{eff}, such that the following holds true:

$$K_{eff} = \frac{F_a}{\Delta_a} \tag{4}$$

In assessment conditions the yield deflection is easily computed and the selected displacement, Δ_a, can be obtained based on the selected performance level or ductility, μ, with:

$$\Delta_a = \mu \Delta_Y \tag{5}$$

Based on the substitute structure shown in Figure 5, the capacity, F_a, at a given μ and for a given post-yield stiffness, r, can be derived based on the relation:

$$F_a = \left[r(\mu - 1) + 1\right]F_y \tag{6}$$

These three equations were used to describe completely the load-deformation response for the substitute structure. This method of converting the structural performance into a simplified response is often designated as the substitute structure approach (Priestley et al., 2000). Meanwhile, the corresponding equivalent elastic period, T_{eff}, is given by:

$$T_{eff} = 2\pi\sqrt{\frac{M}{K_{eff}}} \tag{7}$$

Another parameter that must be used in dynamic analysis using the substitute structure approach is the equivalent viscous damping (EVD) ratio. Previous work (Lu and Silva, 2004) have correlated the EVD ratio, ξ_{eff} , as a function of the displacement ductility level and for members under low or no axial load by the relation:

$$\xi_{eff} = 0.05 + \frac{1}{\pi}\left[1.5 - \frac{1.5 - 0.5r}{\mu} - 0.5r - \frac{r(\mu - 1)}{1 + r(\mu - 1)}\right] \tag{8}$$

Dynamic load effects can be correlated to an equivalent static load by the relation (Clough and Penzien, 1993):

$$DRF = \frac{\Delta_a}{\Delta_{st}} \tag{9}$$

Where D_a is the same as the displacement selected for assessment and the maximum deformation under dynamic loads, and D_{st} is the displacement under static loads, which is given by:

$$\Delta_{st} = \frac{P_s}{K_{eff}} \tag{10}$$

The expression to compute DRF developed for blast loads was given by (Lu and Silva, 2005):

$$DRF = e^{-\frac{\xi_{eff}}{\sqrt{1-\xi_{eff}^2}}\theta^*}\left(f_1 \cos\theta^* + \frac{\xi_{eff} f_1 + f_2}{\sqrt{1-\xi_{eff}^2}} \sin\theta^*\right) \tag{11}$$

Where the θ^* is the phase angle for the maximum displacement given by:

$$\theta^* = \tan^{-1}\left(\frac{f_2\sqrt{1-\xi_{eff}^2}}{f_1 + \xi_{eff} f_2}\right) \tag{12}$$

In the expressions above, f_1 and f_2 are functions of the EVD, ξ_{eff}, and the non-dimensional time duration, t_d / T_{eff}, ratios given by:

$$f_1\left(\xi_{eff}, \frac{t_d}{T_{eff}}\right) = -e^{-2\pi\xi_{eff}\frac{t_d}{T_{eff}}}\left(\begin{array}{l}\left(1+\dfrac{\xi_{eff}}{\pi\dfrac{t_d}{T_{eff}}}\right)\cos\left(2\pi\dfrac{t_d}{T_{eff}}\sqrt{1-\xi_{eff}^2}\right) \\ +\dfrac{1}{\sqrt{1-\xi_{eff}^2}}\left(\xi_{eff}+\dfrac{2\xi_{eff}^2-1}{2\pi\dfrac{t_d}{T_{eff}}}\right)\sin\left(2\pi\dfrac{t_d}{T_{eff}}\sqrt{1-\xi_{eff}^2}\right)\end{array}\right)+\frac{\xi_{eff}}{\pi\dfrac{t_d}{T_{eff}}} \tag{13}$$

$$f_2\left(\xi_{eff}, \frac{t_d}{T_{eff}}\right) = -e^{-2\pi\xi_{eff}\frac{t_d}{T_{eff}}}\left(\begin{array}{l}\left(2\xi_{eff}+\dfrac{4\xi_{eff}^2-1}{2\pi\dfrac{t_d}{T_{eff}}}\right)\cos\left(2\pi\dfrac{t_d}{T_{eff}}\sqrt{1-\xi_{eff}^2}\right) \\ -\dfrac{1}{\sqrt{1-\xi_{eff}^2}}\left(1+\dfrac{\xi_{eff}}{2\pi\dfrac{t_d}{T_{eff}}}\right)\sin\left(2\pi\dfrac{t_d}{T_{eff}}\sqrt{1-\xi_{eff}^2}\right)\end{array}\right)+\frac{1}{2\pi\dfrac{t_d}{T_{eff}}} \tag{14}$$

Using the substitute structure approach for a single degree of freedom system with a given effective stiffness, K_{eff}, and an EVD ratio, ξ_{eff} , correlated to specified damage levels, Figure 6 presents the numerical results for DRF as a function of the non-dimensional time ratio under two different displacement ductility levels (1 and 4). The correlation between these displacement ductility levels and the EVD ratio were obtained in term of Eq. (8). Finally, using the blast load duration ratio, t_d / Te_{ff} , and the DRF obtained from Figure 6 the peak overpressure, P_s, can be determined as:

$$P_s = \frac{\Delta_a K_{eff}}{DRF} \tag{15}$$

Steps Used to Predict the Blast Charge and Standoff Distance

A general flow-chart for predicting the charge weight and the standoff distance is given in Figure 7.

The first step in this procedure consists of selecting the displacement ductility level that will be used in the assessment of the slabs. In this work, the two displacement ductility levels selected for predicting the blast loads were 1 and 4, corresponding to damage levels that can be identified by ”minor cracks or no damage” to “visible cracks

and crushing of the cover concrete". The ductility level selected for assessment of all the corresponding slabs are shown in Table 2. Since the strengthened slabs respond within the elastic range up to failure, the ductility level for these slabs was 1.

Steps 2 through 4 are self explanatory and can be related to the expressions previously described, as shown in Figure 7.

A primary strategy for protecting buildings is to ensure that a certain standoff distance is met such that the shock front generated by explosions decrease significantly with distance. In step 5 the standoff distance, R is selected as shown in the flow-chart, and steps 6 through 9 are once again self explanatory and can be related to the expressions as shown in Figure 7.

In step 10, when the difference between the value of t_d from step 6 and the value of t_{d1} computed in step 10 is within a reasonable degree of accuracy, the procedure is terminated. Otherwise, a new iteration cycle is performed by setting the value of t_d for step 6 as the value of t_{d1} obtained from step 10. Table 2 presents the final iteration and the corresponding steps. The strengthening schemes, materials, experimental test charge weights and the corresponding standoff distances for the five slabs are summarized in Table 3. Detailed research results of the field blast tests is presented and discussed next.

RESULTS AND DISCUSSION

Slab 1 under First Event

The first event was generated by a charge of 0.45 kilogram suspended at a standoff distance of 910mm above the center of the slab, which corresponds to the m=1 damage level. From Figure 8a, it is observed that there was no damage observed on the control slab as expected after this event.

Slab 1 under Second Event

The second event was generated by a charge of 0.9 kilogram at a standoff distance of 300mm above the center of the slab, which corresponds to the m=4 damage level. From Figure 8b, a major flexural crack was observed at the mid-span. The maximum width of the crack was 3mm. The residual displacement at the center of the slab was measured at 21mm, and the residual displacement at the mid-point along the edge was measured at 11mm. By assuming the residual displacement varies linearly from the center to the edges of the slab, the average residual displacement was computed at nearly 14mm. Recognizing the yield displacement equals 4.1mm, the achieved displacement ductility level during test was 4.4, which is close to the predicted displacement ductility level. These results indicate that the charge weight and standoff distance were effectively estimated by using the DBD method.

Slab 2A

An explosive charge of 1.35 kilogram at a standoff distance of 300mm was applied to this slab. As shown in Figure 9a, this slab was severely damaged under this explosive charge, and no residual deformation could be realistically measured. This result indicates that slabs retrofitted by CFRP laminates on one side only are not adequate in increasing the blast-resistant capacity of slabs for the given threat level.

Slab 2B

Slab 2B, was subjected to the same charge weight at the same standoff distance as slab 2A. Two major shear cracks were observed near the supports and no significant flexural crack were observed, as shown in Figure 9b. The measured residual displacement was 44mm and 28mm at the center and the mid span along the edges, respectively. By comparing the experimental test results of slabs 2B with 2A, it can be concluded that the flexural capacity was increased by strengthening on both sides under blast loads. Future testing should also consider the shear failure of retrofitted slabs.

Slab 3A

Slab 3A, was also subjected to a blast load generated by a charge of 1.35 kilogram charge at a standoff distance of 300mm. Figure 10a shows that this slab suffered significant damage under an explosive charge identical to slab 2A. This result indicates that slabs retrofitted by SRP laminates on one side only are also not adequate in increasing the blast-resistant capacity of slabs.

Slab 3B

Slab 3B was also subjected to a blast load generated by a charge of 1.35 kilogram charge at a standoff distance of 300mm. Two major shear cracks were observed near the supports and no significant flexural cracks were observed. The measured residual displacement was 44mm and 28mm at the center and the mid span along the edges, respectively.

CONCLUSIONS

In this work, the blast charge weights and the standoff distance were estimated based on the modified DBD method to impose a desired displacement ductility level. The results of field test for the control slab showed that the achieved displacement ductility levels matched closely the predicted values. Therefore, a primary conclusion drawn from the test results is that the charge weight and standoff distance to generate blast loads can be effectively estimated by the DBD method according to the procedure presented in this paper.

Furthermore, slabs retrofitted on one side only were severely damaged irrespective of the strengthening material. However, slabs retrofitted on both sides were adequate in

resisting the given threat level; but, failure due to the insufficient shear capacity was observed. By comparing the test results of slabs strengthened on one side and on both sides, the main conclusion was that slabs should be retrofitted on both sides in order to make these slabs resistant to realistic blast loads.

ACKNOWLEDGEMENTS

This research program was funded by the National Science Foundation under Grant No. CMS-0335393 and Structural Preservation Systems, through the NSF Industry/University Cooperative Research Center at the University of Missouri - Rolla. In addition the authors would also like to thank Hardwire LLC for their donation of the steel tapes.

REFERENCES

Clough, R.W., and Penzien. J. (1993), *Dynamics of Structures*, 2nd Edition, McGraw Hill Inc., New York, NY, 1993, 635 pp.

Wobbe, E., Silva, P, and Barton, B. et al (2004), "Flexural Capacity of RC Beams Externally Bonded with SRP and SRG" ACI Conference, San Francisco, CA, November, 2004

Federal Emergency Management Agency, (FEMA) (2003) "FEMA 426- Reference Manual to Mitigate Potential Terrorist Attacks Against Buildings" FEMA-426, December 2003.

Hose, Y. D., Silva, P. F., Seible, F. (2000), "Performance Evaluation of Concrete Bridge Components and Systems under Simulated Seismic Loads," *EERI Earthquake Spectra*, Vol. 16, No. 2, May 2000, pp. 413-442.

Longinow, A.; and Alfawakhiri, F. (2003) "Blast Resistant Design with Structural Steel", *Modern Steel Construction*; October 2003 pp. 61-65

Lu, B.; and Silva, P. (2004) "Estimating Equivalent Viscous Damping Ratio For RC Members under different loading Types", *Mechanics Research Communications*; Submitted.

Lu, B.; and Silva, P. (2005) "Inelastic Shock Spectra for Blast Loads", *Mechanics Research Communications*; Submitted.

May, G. C. and Smith, P. D. (1995) *Blast Effects on Buildings*, Thomas Telford Service Ltd, London, E14 4JD. 121pp.

Priestley, M.J.N. (2000), .Performance Based Seismic Design,. *Proceedings of the 12th World Conference on Earthquake Engineering*, Auckland, New Zealand, 2000, State of the Art Paper No. 2831, pp. 325-346.

Priestley, M. J. N., Seible, F., and Calvi, M.,(1995) *Seismic Design and Retrofit of Bridges,* John Wiley & Sons, Inc., New York, NY, Sep 1995, 672 pp.

Table 1 --Material Properties of CFRP and SRP

	Tensile strength (MPa)	Elastic modulus (GPa)	Ultimate strain (%)	Strengthening Area (mm^2)
CRFP	3790	230	1.70	200
SRP	1170	78	2.10	570

Table 2 --Standoff Distance and Estimated Charge Weight of Blast Loads

Step No.	1	2			3	4	5	6	7	8	9	10
Damage level	m	z_{eff} (%)	D_a (mm)	F_a (kN)	K_{eff} (kN/m)	T_{eff} (sec)	R (mm)	t_d (sec)	DRF	P_s (bar)	W (kg)	t_d (sec)
No damage	1	5	4.1	20.5	5040	0.04	910	0.0014	0.110	5.0	0.44	0.0014
Major crack	4	40	16.4	20.5	1260	0.07	300	0.00018	0.005	215	0.91	0.00018
Ultimate (CFRP)	1	5	16.5	133.5	8155	0.03	300	0.00016	0.021	322	1.33	0.00016
Ultimate (SRP)	1	5	16.4	125.5	7718	0.03	300	0.00016	0.020	322	1.30	0.00016

Table 3 --Experimental Test Matrix

Shot No.	Slab No.	Strengthening scheme	Charges Weight (kg)	Standoff Distances (mm)
1	1	None	0.45	910
2	1	None	0.90	300
3	2A	CFRP (1 side)	1.35	300
4	2B	CFRP (2 sides)	1.35	300
5	3A	SRP(1 side)	1.35	300
6	3B	SRP(2 sides)	1.35	300

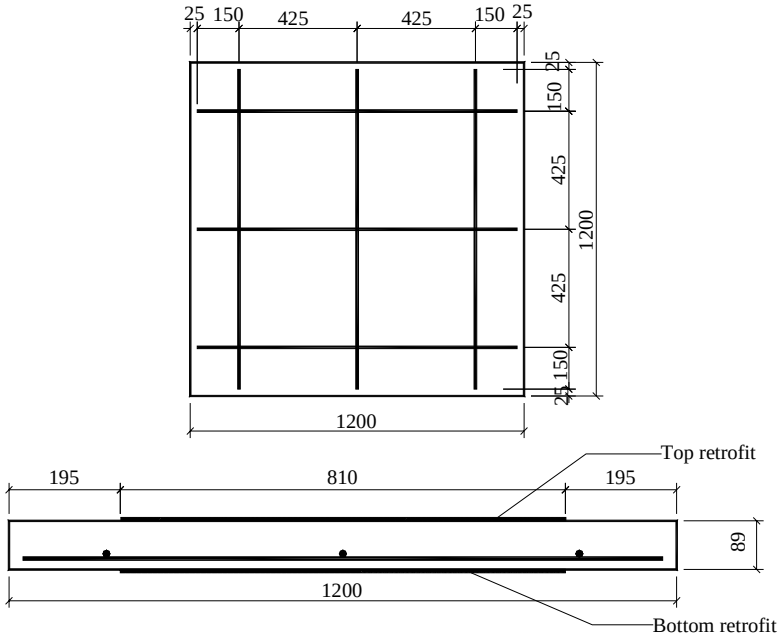

Figure 1 --RC Slab and Reinforcement Detail (in millimeters)

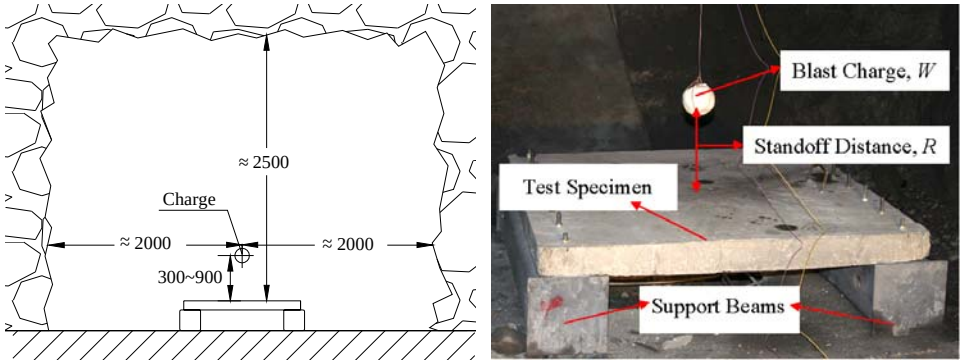

a. UMR Mine Test Site (in millimeters) b. Test Setup

Figure 2 –Test Site and Test Setup

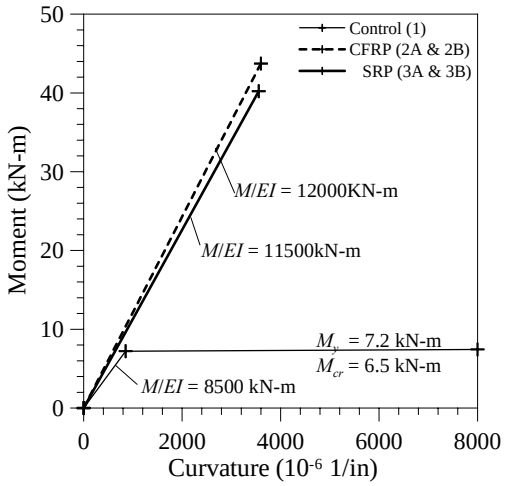

Figure 3 --Moment- Curvature Relationship

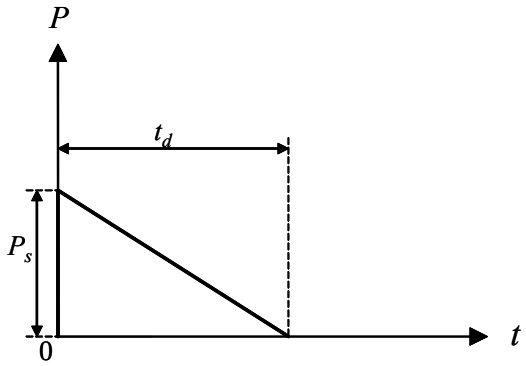

Figure 4 --Simplified Pressure-Time Profile for Blast

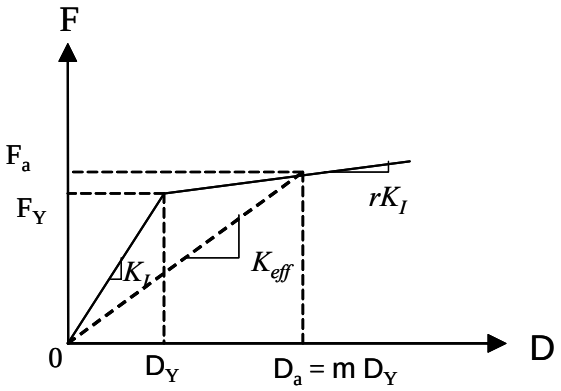

Figure 5 --Substitute Structure Model

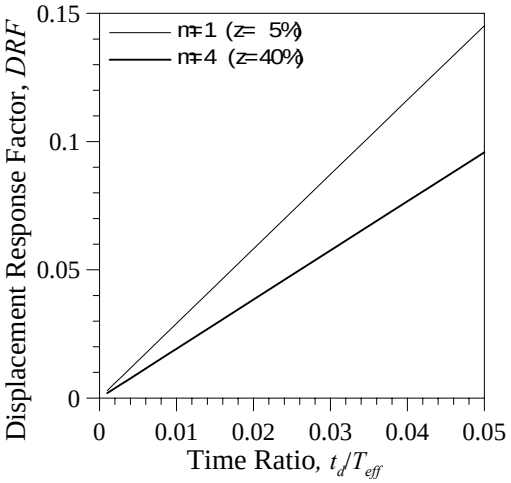

Figure 6 --Displacement Response Factor for Simplified Blast Load

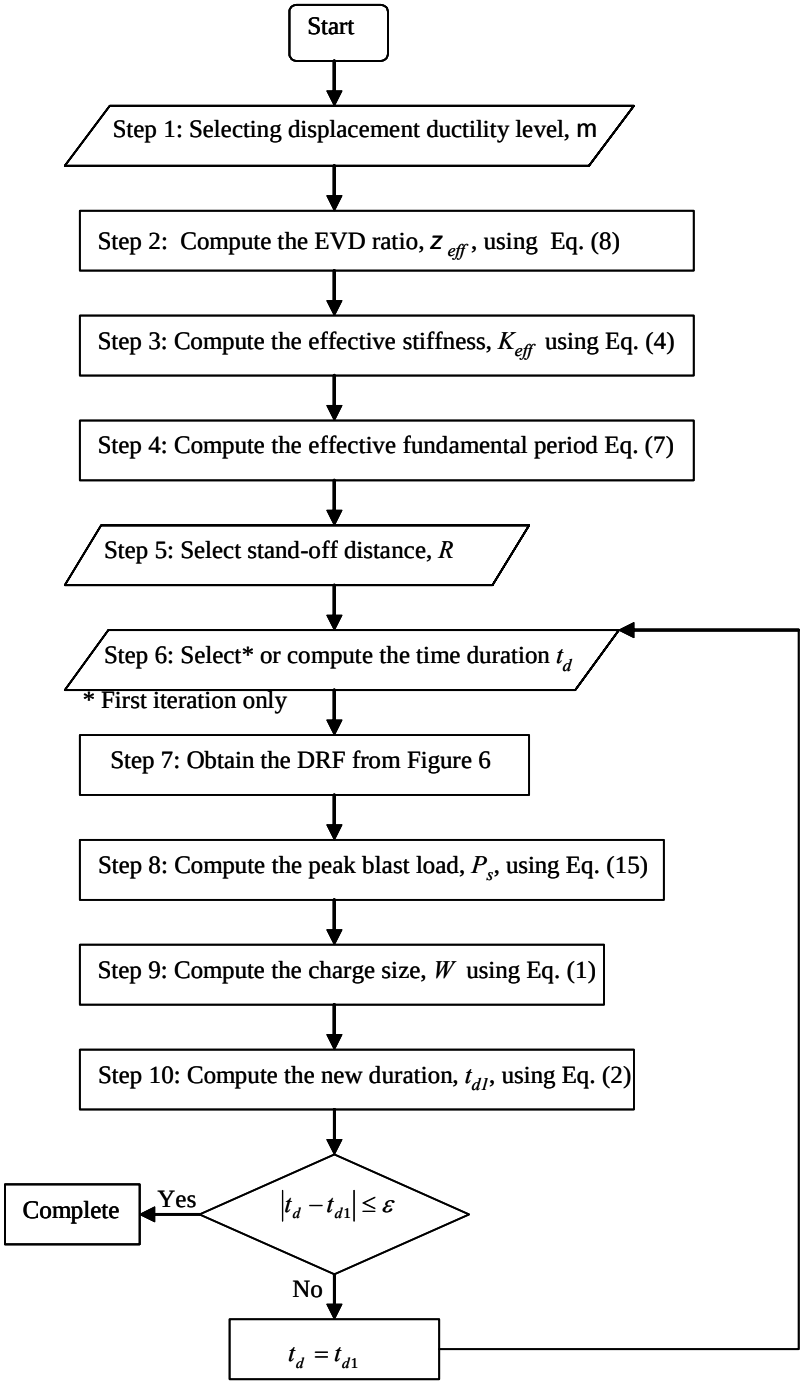

Figure 7 --Flow Chart for Predicting Blast Loads


a. 1st Event (0.45kg, 910mmt) b. 2nd Event (0.9kg, 300mm)

Figure 8 --Test Results for Control Slab


a. 2A (1.35kg, 300mm) b. 2B (1.35kg, 300mm)

Figure 9 --Test Results for CFRP Retrofitted Slabs


a. 3A (1.35kg, 300mm) b. 3B (1.35kg, 300mm)

Figure 10 --Test Results for SRP Retrofitted Slabs)